From Digital Blueprint to Chemical Reality: Methanol to Formaldehyde at Ambient Conditions

Shweta Mehta[a], Mirabai Kasabe[b], Shubhangi Umbarkar*[b,c], Kavita Joshi*[a,c]

[a] *Physical and Materials Chemistry Division, CSIR-National Chemical Laboratory, Dr. Homi Bhabha Road, Pashan, Pune-411008, India.*
[b] *Catalysis Division, CSIR-National Chemical Laboratory, Dr. Homi Bhabha Road, Pashan, Pune-411008, India.*
[c] *Academy of Scientific and Innovative Research (AcSIR), Sector 19, Kamla Nehru Nagar, Ghaziabad, Uttar Pradesh- 201002, India.*

Abstract

Partial oxidation of methanol to value added product presents an intriguing yet challenging process. Among these products, formaldehyde is the simplest and one of the most vital aliphatic aldehydes, which has extensive application across various domains. Industrially, silver and iron-molybdenum oxides are used as catalysts for the conversion of methanol to formaldehyde at elevated temperatures (600°C and 250-400°C, respectively). However, in this computational and experimental study, we have demonstrated the efficacy of ZnO as a catalyst. Notably, in the presence of ZnO, methanol readily converts to formaldehyde even under ambient conditions. We employed periodic density functional theory (DFT) to explore $(10\bar{1}1)$ facet of ZnO to elucidate its interaction with methanol. Our comprehensive analysis identified the most active facet $(10\bar{1}1)$ involved in the spontaneous conversion of methanol to formaldehyde. Subsequently, experimental validation supported our theoretical findings, demonstrating the conversion of methanol to formaldehyde with 100% selectivity at room temperature and atmospheric pressure in the presence of ZnO. This study exemplifies the pivotal role of theory in catalyst design.

Email addresses: `sb.umbarkar@ncl.res.in` (Shubhangi Umbarkar*), `k.joshi@ncl.res.in` (Kavita Joshi*)

1. Introduction

Aldehydes are industrially significant compounds owing to their broad range of applications. Formaldehyde, the simplest aliphatic aldehyde, is of particular interest, due to its applications in diverse sectors including construction, automotive, aviation, pharmaceuticals, and cosmetics.[1] Formaldehyde serves as a crucial raw material in the synthesis of resins, 1,4-butylene glycol, poly formaldehyde, and pesticides, with an annual demand exceeding 30 megatons in recent years.[2] Methanol is a fundamental feedstock for the production of formaldehyde, accounting for over 30% of its annual usage.[3] The conversion of methanol to formaldehyde can occur via either the endothermic dehydrogenation process ($CH_3OH \rightarrow CH_2O + H_2$) or the exothermic partial oxidation process ($CH_3OH + 1/2\ O_2 \rightarrow CH_2O + H_2O$). Industrially two catalysts are used for production of formaldehyde from methanol. One is silver catalyst, in which the methanol and air mixture are subjected to 600^{o}C for formaldehyde production.[4] Another is an iron-molybdenum oxide which works at a relatively lower temperature of 250-400^{o}C.[5] However, both these catalysts are limited by high operational temperature and instability of catalysts at such conditions. Therefore, it is imperative to design a catalyst that can both alleviate the limitations of the previously described industrial catalysts and convert methanol into formaldehyde. Catalysts based on noble metals, viz. Pt[6–9] and Pd[10, 11] have been extensively explored for their catalytic activity towards MeOH conversion to HCHO. In a recent investigation, Selivanova et al. demonstrated the oxidation mechanism of methanol on Pt(111) single crystal utilizing X-ray photoelectron spectroscopy (XPS) and polarization-modulation infrared reflection absorption spectroscopy (PM-IRRAS).[9] They illustrated that on a Pt surface, complete oxidation of methanol is preferred over partial oxidation, which begins at 350K. As a result, the primary products are CO_2 and methyl formate, while formaldehyde is produced only in trace amounts within the temperature range of 350-450K. Although, use of bulk Pt catalyst exhibits limited effectiveness in facilitating the partial oxidation of methanol to formaldehyde, supported catalyst with substantially less amount of Pt shows better activity for partial oxidation of methanol. In an experimental study, Nalajala et al. explored various catalyst configurations involving Pd and Pt supported on TiO_2 for partial oxidation of methanol.[11] They observed that the most effective conversion of methanol to formaldehyde (0.2μmol/h.mg) occurred when 0.5 monolayer of Pt was coated on the Pd nanocubes supported on TiO_2. The introduction of Pt onto Pd significantly enhanced the catalytic activity on the Pt(111) facet. Interestingly, this enhanced catalytic activity was achieved with less than one monolayer of Pt, contrasting with the performance of bulk Pt. Marcinkowski et al. used another approach by employing a single-atom catalyst (SAC) composed of Pd on Fe_3O_4(0001) for the partial oxidation of methanol to formaldehyde.[10] They observed that on Fe_3O_4(0001), methanol converts to formaldehyde at 516K, whereas on Pd_1/Fe_3O_4(0001), the conversion occurs at 290K. However, the introduction of methanol commences the sintering process of Pd at temperatures as low as 300K, leading to the formation of Pd clusters that hinder the conversion of methanol to formaldehyde. Notably, the viability of single-atom catalysts is governed by the stability of the catalyst under the reaction temperature conditions. Although, tailoring the structure, and morphology of these metals resulted into enhanced efficiency, the use of precious metals as catalysts imposes limitations on their applications.

Introduction of oxygen on the metal surfaces greatly affect their catalytic activity. Presence of oxygen affects the strength of adsorption of the adsorbate/intermediates, simultaneously altering the charge density distribution on the surface. In our recent investigations, we have delved into the interactions of methanol with both metallic Zn and oxygen-pre-adsorbed Zn surfaces.[12] We demonstrated that a notable decrease in the activation barrier occurs for methanol dissociation upon oxygen pre-adsorption on metallic surfaces compared to their non-preadsorbed counterparts. Metal oxides exhibits better catalytic activity as compared to the metals due to the presence of distinct sites (cationic and anionic) at the oxide surface.[13–18] Literature is abundant with studies that discusses the metal oxides explored for the partial oxidation of methanol.[13, 14, 19–23] Earth abundant, hence cost effective ZnO has received considerable attention for the interaction with methanol.[16, 24–28] Few DFT studies have shown that on the polar, zinc-terminated (0001) surface, the adsorption of dissociated methanol is more stable than that of molecularly adsorbed methanol.[25, 29] Deng et al. conducted a comparison between the activation of methanol on ZnO(0001) bilayer and bilayer-trilayer stepped surfaces supported on Au(111) using temperature-programmed reaction spectroscopy (TPRS) and DFT analysis.[16] Their studies elucidate that the ZnO bilayer exhibited inertness towards methanol oxidation, with molecular desorption occurring at 220K and 260K in TPRS. In contrast, the ZnO bilayer-trilayer setup demonstrated molecular desorption of methanol at 380K, followed by formaldehyde desorption at 580K in TPRS. Furthermore, the minimum activation barrier calculated through the DFT was determined to be 19.0 kcal/mol for the ZnO bilayer-trilayer configuration. However, polar surfaces undergo substantial reconstructions and are unlikely to occur in the truncated-bulk ZnO structure.[30] On the contrary, nonpolar, mixed-terminated ZnO surfaces can preserve their undecorated and largely unreconstructed truncated-bulk form,[31] offering both acidic and basic sites simultaneously for the adsorption of dissociated fragments. Therefore, thorough understanding of the interaction of methanol with non-polar surfaces of ZnO stands out as a rational choice. On the nonpolar $(10\overline{1}0)$ facet of ZnO, molecular adsorption of methanol is energetically stable than its dissociation, this has been evidently acclaimed by various theoretical studies.[24, 26–28] Abedi et al. computed the dissociation barrier for the O-H bond of methanol as 0.5 eV by employing DFT.[27] In our previous study, we demonstrated that on step facets of ZnO ($(10\overline{1}3)$ and $(11\overline{2}2)$ spontaneous dissociation of O-H bond of methanol takes place and is energetically more favorable than the molecular adsorption.[28]

While ZnO has been extensively investigated in terms of its interaction with methanol, the complex surface structure of ZnO and qualitative differences between its various exposed crystal facets make the unambiguous determination of the local atomistic structure at reaction sites and the involved mechanism a formidable task. In this study, we discuss an unexplored nonpolar, mixed-terminated $(10\overline{1}1)$ facet of ZnO and its interaction with methanol. We first discuss the theoretical results that shows spontaneous conversion of methanol to formaldehyde followed by the rationale why it works. Further, we present the experimental results that validates our theoretical predictions and demonstrate the conversion of methanol to formaldehyde at room temperature and atmospheric pressure. This study illustrates the importance of theoretical approaches in the rational design of catalysts.

2. Methodology

2.1. Computational Details

All the calculations were carried out within the Kohn-Sham formalism of density functional theory. Projector Augmented Wave potential [32, 33] was used, with Perdew-Burke-Ernzerhof (PBE) approximation for the exchange-correlation and generalized gradient approximation, [34] as implemented in plane-wave, pseudopotential based code, Vienna Ab initio Simulation Package (*VASP*).[35–37] The bulk unit cell was taken from the materials project.[38] The bulk lattice parameters upon optimization were a = 3.28Å and c = 5.30Å which were in excellent agreement with the experimentally measured (a = 3.24Å, c = 5.20Å) lattice parameters.[39, 40] The flat facet, $(10\overline{1}1)$ of ZnO was modeled as a slab by cleaving a surface with 3x3 periodicity in x and y direction with four layers using Quantumwise-VNL-2017.1.[41] The bottom layer was fixed, and the rest all layers and adsorbate were fully relaxed for all the surface calculations. Van der Waals corrections were applied to account dynamic correlations between fluctuating charge distribution by employing the Grimme method (DFT-D2).[42] It was observed that 20 Å of vacuum was sufficient to avoid interaction between adjacent images of planes along the z-direction. Geometry optimization was carried out with a force cutoff of 0.01 eV/Å on the unfixed atoms and the total energies converged below 10^{-4} eV for each SCF cycle. A Monkhorst-Pack grid of 3x2x1 for $(10\overline{1}1)$ slab was used. The energy difference was less than 3meV/atom upon using finer mesh. Entire surface was scanned by placing the MeOH molecule at all available unique sites. The interaction energy was calculated using the formula: $E_{int} = E_{system}$ - ($E_{surface} + E_{molecule}$) where E_{system} was the energy of the system when MeOH was placed on the surface, $E_{surface}$ was the energy of the bare surface and $E_{molecule}$ was the energy of the MeOH molecule. To understand the underlying electronic structure total Density of States (*tDOS*) was calculated with denser k-mesh using LOBSTER.[43–46]

2.2. Experimental methods

Preparation of catalyst All the reagents such as zinc acetate, sodium hydroxide, methanol, and ethanol of AR grade quality, were procured from Molychem India, and Thomas Baker Chemicals, India and used as such without further purification. The ZnO nanoparticles were synthesized using precipitation method.[47] 20 mL of an aqueous solution of 6 mmol $(CH_3COO)_2Zn.2H_2O$ was added to a beaker. Further 10 mL of 20 mmol NaOH was added dropwise to the aqueous zinc acetate solution and stirred. Then, the produced precipitate was kept at 70^{o}C for 15 h. The prepared catalyst was cooled at room temperature, filtered and followed by rinsing with a mixture of H_2O:C_2H_5OH (70:30), and dried at 70^{o}C for 10 h before using in the experiments.

Catalyst characterization

The prepared catalyst was characterized by the X-ray diffraction method using PAN analytical X"Pert Pro Dual Goniometer diffractometer. The diffractometer consists of X$'$celerator solid-state detector with CuKα (λ = 1.5406Å , 40kV, 30mA) radiation and a Ni filter. The X-ray diffraction pattern of the sample was collected in the range of 2θ = 20-80^o with a step size of 0.02^o and a scan rate of 4^{o}min^{-1}. Further, morphology of the catalyst was determined using scanning electron microscopy (SEM) on a FEI quanta 200 3D dual beam ESEM instrument having thermionic emission tungsten filament in the 3 nm range at 30 kV.

Catalytic activity The catalytic oxidation of methanol to formaldehyde was carried out in a 5 ml glass vial at room temperature. 2 g methanol and 25 wt% catalyst were added into the vial. After addition, the vial was closed and the reaction mixture was stirred for 1h. Fourier Transform Infrared Spectroscopic studies (FTIR) of the reaction mixtures were carried out using a Thermo Nicolet Nexus 670 IR instrument using DTGS detector to analyze the products formed due to oxidation of methanol. KBr pellet method was used to prepare samples with a resolution of 4 cm^{-1} in the range of 4000-400 cm^{-1} averaged over 100 scans.

High performance liquid chromatography (HPLC, Agilent technologies, modal 1250 infinity) was used to analyze the liquid samples to identify the products. HPLC equipped with an RI detector (at 40^oC) and H^+ Aminex column (305 x 7.8 mm^2) fitted with a guard column in series was used. The mobile phase used was 0.05M H_2SO_4 at a flow rate of 0.6 mL/min while maintaining the column temperature at 60^oC. Quantitative analysis of the products was carried out with that of the reference samples with known concentrations using calibration method.

Micro Gas chromatography (Agilent technologies, 490 micro GC- quad w/ four channels) was used for identification of any gaseous products formed during the reaction. The micro GC is equipped with four columns micro-thermal conductivity detector (μ TCD). The first channel is equipped with a 10 meter CP-MolSieve 5Å column, running on argon as carrier gas. Second channel is equipped with 10 meter long PoraPLOT U column, third channel has PLOT Al_2O_3/KCl column and fourth channel is equipped with 8 meter long 5CB column. Channels 1-3 have backflush functionality. Each sample was injected 5 times to eliminate the contamination and the last 3 runs are used for quantitative analysis.

3. Results and discussion

Designing a catalyst for the selective oxidation of methanol is a challenging yet intriguing due to competing pathways for complete oxidation. The condition for selective oxidation is the optimal adsorption of reactants/intermediates and effective desorption of the desired products to reduce the probability of further oxidation. In our previous work, we investigated the interaction of methanol with four different facets of ZnO and observed both molecular adsorption and spontaneous dissociation of methanol on different facets.[28] By a detailed analysis of the inherent electronic structure of these facets, we shed light on why a particular facet of ZnO exhibit preference for methanol dissociation. Notably, the existence of energy states at Fermi level plays a crucial role in facilitating methanol dissociation on a given facet.

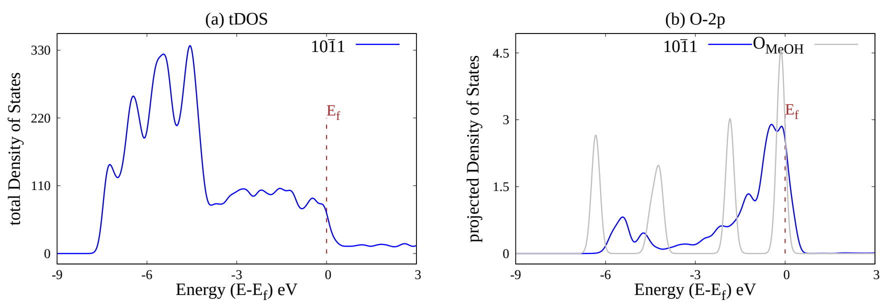

Figure 1: (a) shows the $tDOS$ of ($10\bar{1}1$) facet. (b) shows the $2p$ of a representative surface oxygen atom (blue) and gaseous methanol molecule (gray). The presence of energy states at Fermi level is evident from the plots.

($10\bar{1}1$) is another non-polar flat facet of ZnO, whcih was not explored in our previous study. To begin, we investigated the underlying electronic structure of bare ($10\bar{1}1$) facet by ploting density of states (refer to Fig.1). Total density of states plot is depicted in Fig.1-(a), distinctly indicates the energy states at the Fermi level. Furthermore, Fig.1-(b) illustrates the projected density of states for the $2p$ of a representative surface oxygen atom. The reference pDOS for the $2p$ of O_{MeOH} is depicted in Fig.1-(b) as a gray curve. Notably, the energy states present at the Fermi level for the surface oxygen atom coincide with the $2p$ states of O_{MeOH}. This phenomena proposes the ($10\bar{1}1$) facet to be an active one for the dissociation of methanol.

To demonstrate this, we investigated the interaction of methanol with the

Table 1: Interaction energy (eV), O-H bond-length (Å), C-O bond-length (Å), and Zn-O_{MeOH} bond-length (Å) for various sites on ZnO ($10\overline{1}1$) facet. All these positions are indicated in Fig.1-(b). Dissociation is indicated in red color while molecular adsorption is shown in black color.

Positions	E_{int} (eV)	O-H BL (Å)	C-O BL (Å)	Zn-O_{MeOH} BL (Å)
4	-7.95	3.23	1.23	3.34
1	-4.44	0.98	1.45	2.30
5	-3.17	0.98	1.45	2.27
7	-2.66	1.65	1.41	2.03
3	-1.82	0.98	1.43	2.57
6	-1.75	0.99	1.42	3.55
2	-1.66	0.98	1.42	3.73

($10\overline{1}1$) facet. This facet is a mixed-terminated facet having both oxygen and zinc on the surface. Zn atoms in the bulk layer are coordinated to four oxygen atoms while the Zn atoms in the surface layers are only coordinated to three oxygen atoms. The top and side view of the ($10\overline{1}1$) facet is shown in Fig. SI1. Methanol was placed at various unique sites on the facet such as on top of Zn, bridge of two Zn, bridge of Zn and O, bridge of two O. All the sites where MeOH was placed are shown schematically in Fig. SI2. The numbers in Fig. SI2-(a) represent the initial positions where MeOH was placed and final position of adsorbed methanol or dissociated methoxy group are shown in Fig. SI2-(b). The black numbers indicate molecular adsorption while the red numbers denote dissociation of methanol. The interaction energy of MeOH adsorption, O-H bond-length, C-O bond-length, Zn-O_{MeOH} are reported in Tab.1.

We observed the spontaneous decomposition of methanol to formaldehyde at ($10\overline{1}1$) facet of ZnO. Among all possible outcomes, the formation of formaldehyde is thermodynamically the most favorable outcome of the interaction of

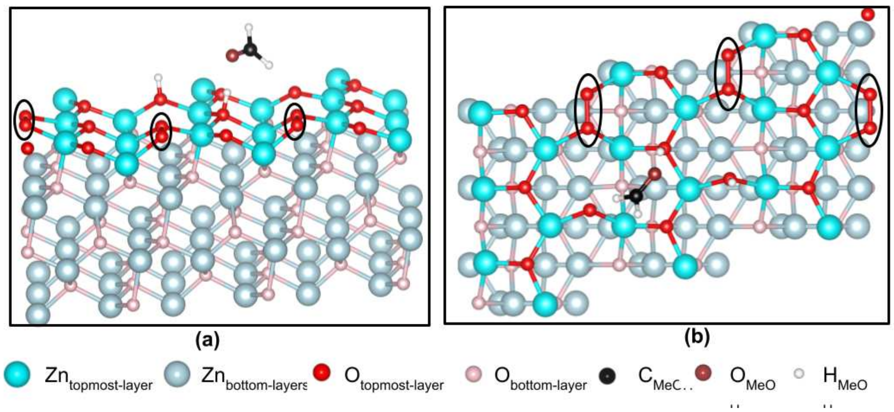

Figure 2: Methanol decomposes to formaldehyde at ZnO ($10\overline{1}1$) facet. (a) depicts side view, and (b) shows the top view of slab with formaldehyde formed. The dissociated H atoms adsorb at two different O_{surf} atoms. O-O dimers are formed at the ZnO surface.

methanol with this facet, as shown in Tab.1. However, as seen from the Tab.1, the formation of other products from MeOH is improbable because of the substantially significant energy difference (>3.50 eV) between formaldehyde formation and other outcomes. The C-O and C-H bond-lengths of the produced formaldehyde were 1.23Å and 1.11Å respectively, similar to the bond-lengths in isolated formaldehyde molecules (C-O = 1.22Å ; C-H = 1.10Å). We also computed the vibrational frequency of this produced formaldehyde. The C=O bond stretching vibration frequency was 1713.23 cm^{-1}, comparable to an isolated formaldehyde molecule (1778.97 cm^{-1}). The dissociated hydrogen atoms adsorbed at two different surface oxygen atoms, as shown in Fig.2. Interestingly, surface reconstruction occurred upon decomposition of methanol which leads to formation of O-O dimer on the surface, as shown in black circles in Fig.2. Bond-length of these newly formed O-O dimers varies between 1.43-1.45Å, and is comparable to O-O bond-length in peroxides.

The formation of formaldehyde at ZnO is peculiar to this facet. Since the availability of energy states at Fermi explains the dissociation of O-H bond, however, spontaneously dissociation of C-H bond is certainly intriguing. To understand the difference in behaviour of interaction with methanol on these

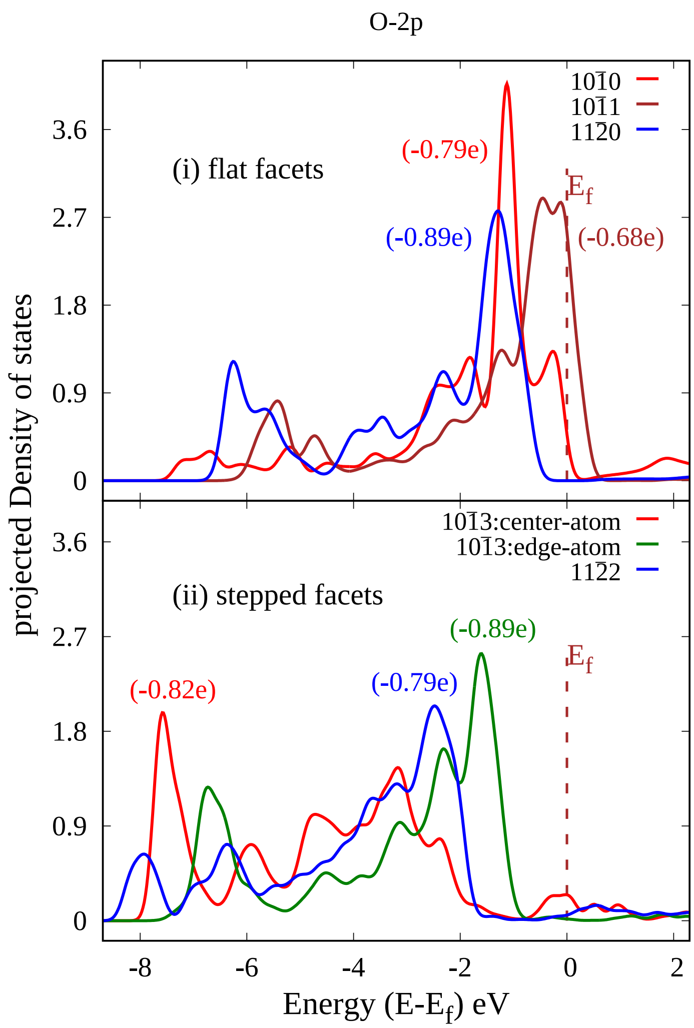

Figure 3: *pDOS* of 2p of oxygen on all the facets of ZnO investigated in previous and current work (10$\bar{1}$1). It is evident from the plot that oxygen of (10$\bar{1}$1) facet has empty states above the Fermi level. It signifies the unsaturation of oxygen on this facet and their easy availability for abstracting two hydrogens from MeOH.

Table 2: Coordination number, Mulliken charges of Zn and O atom of the top most layer of ZnO facets are shown. Facets studied in previous work[28] are marked in blue

Surface	Co. no. of Zn	Mulliken charge on Zn	Co. no. of O	Mulliken charge on O
$10\bar{1}0$	2	0.85	2	-0.79
$11\bar{2}0$	3	0.96	3	-0.89
$10\bar{1}3$	3(2)	0.96(0.64)	3	-0.89(-0.82)
$11\bar{2}2$	2	0.81	3	-0.85
$10\bar{1}1$	4	1.04	2	-0.68

different facets, we carefully compared the nature of oxygen on the surface in all the facets of ZnO investigated in current and previous work. Coordination number and Mulliken charges of surface oxygen of all facets are reported in Tab.2. Oxygen atoms present at ($10\bar{1}1$) are having least charge (-0.68e) and hence are readily available for the abstraction of hydrogen from MeOH. The comparative $pDOS$ of $2p$ of oxygen on all facets is shown in Fig.3. It is evident from the plot that oxygen of ($10\bar{1}1$) facet has empty states above the Fermi level. It signifies the unsaturation of oxygen on this facet and their easy availability for abstracting two hydrogens from MeOH.

Further, we have also increased the methanol molecule on the surface to explore the effect of increasing monolayer concentration on the interaction. We placed two MeOH molecules in the vicinity of the unstaurated oxygen. Similar to the outcome of one molecule, here also both MeOH molecules dissociates to formaldehyde and desorb from the surface as shown in Fig.4. The O-O peroxide dimer formation is also consistent with increasing monolayer concentration and the dissociated hydrogen adsorb to the surface oxygen atoms.

Apart from formaldehyde formation, methanol either physisorbs, chemisorbs

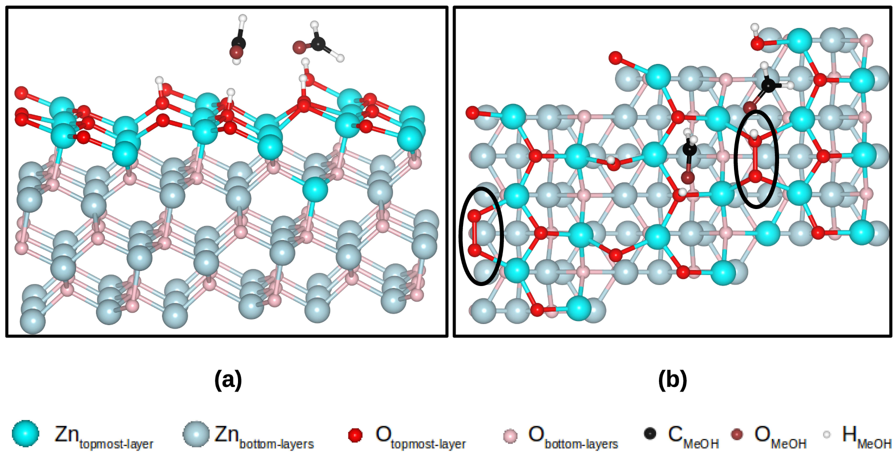

Figure 4: When 2 molecules of methanol are placed at $(10\overline{1}1)$ facet. Both of them dissociate to formaldehyde and desorb from the surface. (a) shows the side view of 2 formaldehyde formed on the surface. (b) shows the top view of the slab. Here also, O-O dimers formed on the surface marked in black circles.

or dissociates on the surface as shown in Fig. SI3. In the case of physisorption (Fig. SI3-(a)), MeOH is adsorbed at the surface with minimal elongation in O-H bond-length (0.98Å). For chemisorption, MeOH adsorbs via its O atom at surface Zn atom with an O-H bond elongated upto 0.99Å (represented in Fig. SI3-(b)). MeOH dissociates on the surface with methoxy and H atom adsorbed at surface Zn and O atom respectively (refer Fig. SI3-(c)).

Based on our theoretical results, we designed an experiment to study the reaction of methanol with ZnO catalyst which is discussed in the following section.

3.1. Catalyst characterization

3.1.1. XRD analysis

The ZnO nanoparticles are prepared by the precipitation method and the XRD pattern for these nanoparticles shows sharp peaks as depicted in Fig.5. The sharpness of XRD peaks is ascribed to the synthesized material consisting of nano-scale particles. Sharp peaks at 31.73^o, 34.45^o, 36.16^o, 47.45^o,

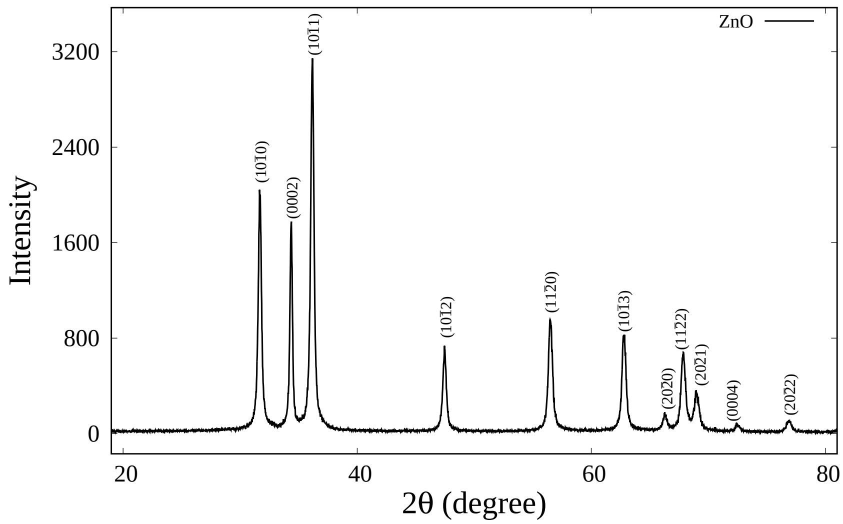

Figure 5: XRD pattern of as-synthesized ZnO. The most prominent peak is (10$\overline{1}$1).

56.49^o, 62.84^o, 66.35^o, 68.1^o, 69.2^o, 72.05^o, and 77.13^o corresponding to the following lattice planes (hkl) of wurtzite polycrystalline structure of ZnO are (10$\overline{1}$0), (0002), (10$\overline{1}$1), (10$\overline{1}$2), (11$\overline{2}$0), (10$\overline{1}$3), (20$\overline{2}$0), (11$\overline{2}$2), (20$\overline{2}$1), (0004), and (20$\overline{2}$2), respectively (JCPDS card No. 36-1451). The spectrum does not contain any characteristic peak except ZnO peaks, which corroborates towards purity of the synthesized material. The particle size has been calculated using Debye-Scherrer formula $D = 0.89\lambda \ / \ \beta \cos\theta$ where, 0.89 is Scherrer's constant, λ is the wavelength of X-rays, θ is Bragg's diffraction angle, and β is the full width at half-maximum (FWHM) of the diffraction peak corresponding to the plane. The calculated particle size is 22 nm, by considering the FWHM of intense peak located at 36.16^o which is attributed to the (10$\overline{1}$1) plane.

3.1.2. Scanning electron microscopy (SEM) analysis

SEM and energy dispersive X-ray (EDX) analysis are carried out to understand the morphology and elemental composition of synthesized ZnO nanoparticles. The SEM images of synthesized ZnO nanoparticles are recored at 10μm and 3μm resolution as shown in Fig.6-(a) and Fig.6-(b) respectively. The ZnO

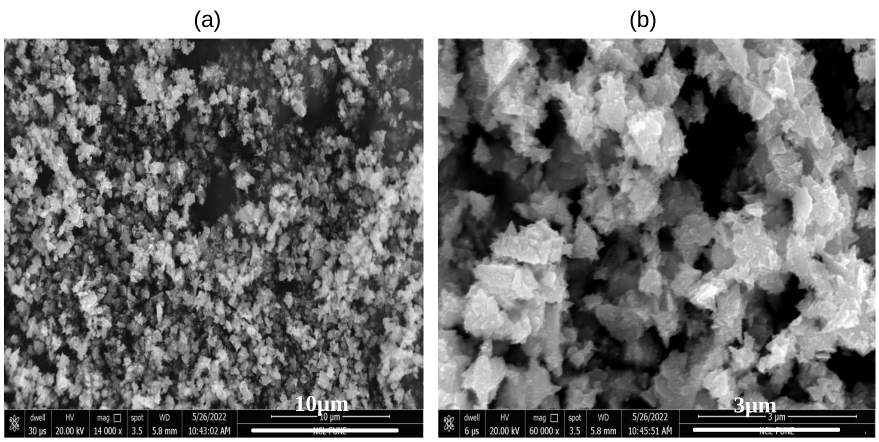

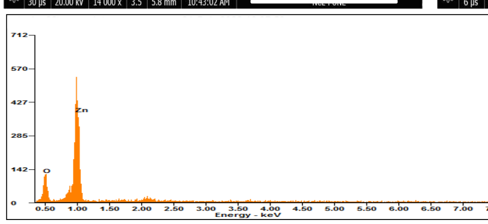

Element	Wt%	At%
OK	25.04	57.71
ZnL	74.96	42.29

(d)

Figure 6: SEM images of ZnO nanoparticles at (a) 10 μm and (b) 3 μm resolution. The image shows irregular and triangular shaped ZnO nanoparticles. (c) and (d) shows EDX analysis of ZnO nanoparticles.

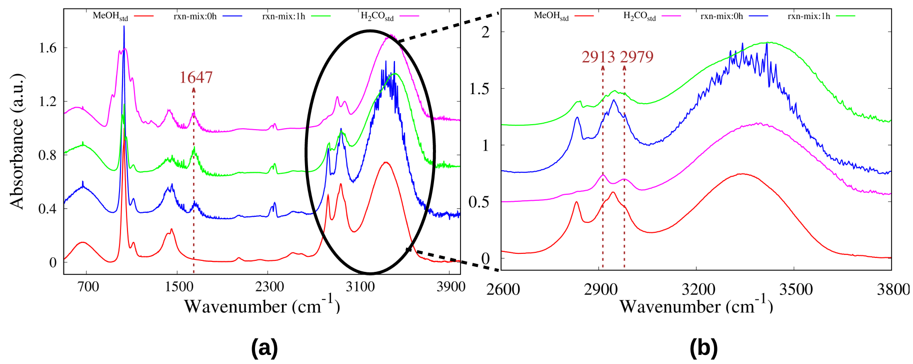

Figure 7: FTIR spectrum of standard methanol, standard formaldehyde, reaction mixture at 0 minute, reaction mixture at 1 h are shown. (a) shows the carbonyl peak corresponds to 1647 cm^{-1} coinciding with standard formaldehyde. (b) shows two tiny peaks appearing at 2913 and 2979 cm^{-1} in the reaction mixture at 0 min and 1 h. These peaks correspond to C-H vibrations in formaldehyde.

nanoparticles are found to be irregular in size and triangular shaped, which is in line with the previous literature.[48] We also observed formation of clusters in the nanoparticles due to agglomeration of particles. EDX analysis confirmed the presence of only zinc (74.96%) and oxygen (25.04%) elements. This attributes to the absence of impurity in the synthesized ZnO nanoparticles.

3.2. Catalytic activity

To investigate the interaction of methanol with ZnO nanoparticles, we performed the reaction at ambient conditions (i.e. RT and atmospheric pressure). The reaction mixture is analyzed after an hour using FTIR and HPLC. Our theoretical results show the formation of formaldehyde as a product of MeOH interaction with ZnO. And hence we have compared our reaction mixture with standard formaldehyde in both FTIR and HPLC. (considering our expected outcome as formaldehyde)

3.2.1. FTIR analysis

We recorded the FTIR spectra of reaction mixtures to analyze the products formed at 0 min. (after the addition of catalyst in methanol) and 1 h. We have compared this data with pure methanol and formaldehyde spectrum. The FTIR spectra of standard methanol, standard formaldehyde, and reaction mixture at 0 min and 1 h are shown in Fig.7. IR spectrum of pure methanol shows various vibrational peaks associated with bending of C-O-H at 1447 cm^{-1}, stretching of O-H at 3338 cm^{-1}, stretching of C-O at 1020-1112 cm^{-1} and stretching of C-H at 2830 and 2941 cm^{-1} (refer Fig.7-(a)). The IR spectrum of reaction mixture at 0 min showed the emergence of peak at 1647 cm^{-1} (blue color peak in Fig.7-(a)), which can be attributed to carbonyl peak in formaldehyde (pink colored peak in Fig.7-(a)). We also observed presence of two tiny peaks at 2913 and 2979 cm^{-1}, which corresponds to C-H peak in formaldehyde (refer Fig.7-(b)). Increase in the intensities of the peaks for C-O and C-H vibrations in 1h reaction mixture signifies the further conversion of methanol to formaldehyde (as shown in green colored peak in Fig.7-(a)).

3.2.2. Chromatographic analysis

We performed HPLC analysis to validate the presence of formaldehyde as the product in the reaction mixture. The reactant (methanol) and expected outcome (formaldehyde) with known concentration and reaction mixture (at 1 hr) are subjected to the HPLC analysis under identical conditions. The results are shown in Fig. SI4. It is evident from the Fig.SI4 that a new peak appears (apart from methanol) in the reaction mixture at 1 hr as shown in Fig. SI4. This new peak coincides with the standard formaldehyde peak in Fig. SI4-(b). Interestingly, there are no other peaks for side products that indicate 100% selectivity for formaldehyde.

To explore the effect of temperature on the methanol oxidation to formaldehyde, the reaction was carried out at RT ($\sim 30^oC$), 80^oC and 100^oC as shown in Fig.8-(a). Formaldehyde yield increases with increasing temperature from 0.36μmol/h.mg to 1.29μmol/h.mg to 1.95μmol/h.mg respectively at 10% catalyst loading. Also, to understand the impact of catalyst loading on the reaction, we varied the relative ratio of catalyst to methanol and performed the reaction at 100^oC. The catalyst loading vs. yield of formaldehyde is plotted in Fig.8-(b). It

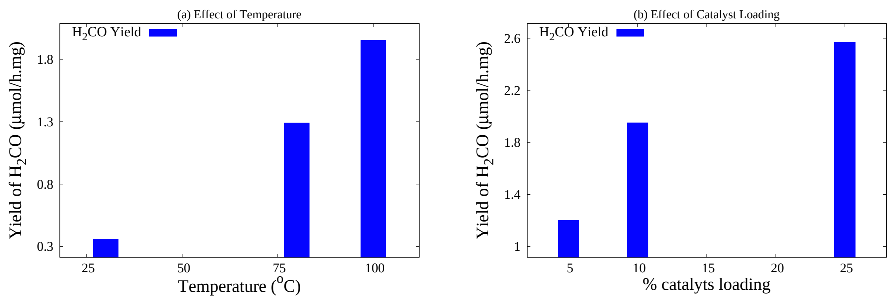

Figure 8: (a) Effect of temperature on the yield of formaldehyde production at ZnO catalyst at 10% catalyst loading. (b) shows the effect of catalyst loading on the yield of formaldehyde produced at 100^{o}C. The yield of formaldehyde increases as a function of both temperature and catalyst loading.

is evident from the plot, that increasing the catalyst loading favors the reaction to proceed. Increasing the catalyst concentration leads to higher availability of the active site and hence increase in the product yield.

Continual efforts are ongoing to engineer catalysts with improved environmental sustainability compared to the existing ones. The rational design of catalysts requires an understanding of molecule-surface interactions and the extraction of pivotal factors influencing desired product formation. DFT serves as a computational method that offers detailed and accurate descriptions of catalytic reactions occurring on surfaces, enabling meaningful comparisons between computational predictions and experimental observations.

We further validated our predicted results with experiments and observed formaldehyde formation from methanol at ambient conditions.

4. Conclusion

In summary, our investigation delved into the interaction of methanol with the $(10\bar{1}1)$ facet of ZnO by employing periodic DFT. Our theoretical findings propose that on this facet, methanol undergoes spontaneous conversion to formaldehyde and subsequently desorbs from the surface, effectively addressing challenges associated with byproduct formation. The presence of highly unsaturated surface oxygen facilitates the dissociation of both O-H and C-H bonds of methanol. Electronic structure analysis suggests a one-to-one correlation between the characteristics of the bare facet and the outcomes of its interaction with methanol.

To validate our theoretical findings, we conducted experimental studies investigating the interaction of methanol with ZnO under ambient conditions. Both FTIR and HPLC analyses corroborate the formation of formaldehyde as the primary product of this reaction. Notably, the absence of peaks other than formaldehyde in the reaction mixture indicates 100% selectivity of formaldehyde under these conditions.

The fundamental goal of computational studies is to discern trends and enhance predictive capabilities through the interpretation of results in the context of the underlying electronic structure. This investigation marks a step towards the efficient design of catalysts.

5. acknowledgement

CSIR-4PI is gratefully acknowledged for the computational facility.

References

[1] B. Elvers, Ullmann's encyclopedia of industrial chemistry, Vol. 17, Verlag Chemie Hoboken, NJ, 1991.

[2] L. E. Heim, H. Konnerth, M. H. G. Prechtl, Future perspectives for formaldehyde: pathways for reductive synthesis and energy storage, Green Chem. 19 (2017) 2347–2355.

[3] A. M. Bahmanpour, A. Hoadley, A. Tanksale, Critical review and exergy analysis of formaldehyde production processes, Reviews in Chemical Engineering 30 (6) (2014) 583–604.

[4] M. Karatok, M. G. Sensoy, E. I. Vovk, H. Ustunel, D. Toffoli, E. Ozensoy, Formaldehyde selectivity in methanol partial oxidation on silver: Effect of

reactive oxygen species, surface reconstruction, and stability of intermediates, ACS Catalysis 11 (10) (2021) 6200–6209.

[5] S. Deshmukh, M. van Sint Annaland, J. Kuipers, Kinetics of the partial oxidation of methanol over a Fe-Mo catalyst, Applied Catalysis A: General 289 (2) (2005) 240–255.

[6] Z. Chen, Y. Mao, J. Chen, H. Wang, Y. Li, P. Hu, Understanding the dual active sites of the FeO/Pt(111) interface and reaction kinetics: Density functional theory study on methanol oxidation to formaldehyde, ACS Catalysis 7 (7) (2017) 4281–4290.

[7] L. Tao, Y. Shi, Y.-C. Huang, R. Chen, Y. Zhang, J. Huo, Y. Zou, G. Yu, J. Luo, C.-L. Dong, S. Wang, Interface engineering of Pt and CeO_2 nanorods with unique interaction for methanol oxidation, Nano Energy 53 (2018) 604–612.

[8] H. Li, X. Wu, X. Tao, Y. Lu, Y. Wang, Direct synthesis of ultrathin Pt nanowire arrays as catalysts for methanol oxidation, Small 16 (33) 2001135.

[9] A. V. Selivanova, V. G. Demina, E. E. Aydakov, A. A. Saraev, V. V. Kaichev, V. I. Bukhtiyarov, Mechanistic study of methanol oxidation on Pt(111) single crystal, Applied Surface Science 579 (2022) 152140.

[10] M. D. Marcinkowski, S. F. Yuk, N. Doudin, R. S. Smith, M.-T. Nguyen, B. D. Kay, V.-A. Glezakou, R. Rousseau, Z. Dohnálek, Low-temperature oxidation of methanol to formaldehyde on a model single-atom catalyst: Pd atoms on Fe_3O_4(001), ACS Catalysis 9 (12) (2019) 10977–10982.

[11] N. Nalajala, K. N. Salgaonkar, I. Chauhan, S. P. Mekala, C. S. Gopinath, Aqueous methanol to formaldehyde and hydrogen on Pd/TiO_2 by photocatalysis in direct sunlight: Structure dependent activity of nano-pd and atomic pt-coated counterparts, ACS Applied Energy Materials 4 (11) (2021) 13347–13360.

[12] S. Mehta, K. Joshi, Electronic fingerprints for diverse interactions of methanol with various Zn-based systems, Surface Science 736 (2023) 122350.

[13] G. S. Wong, D. D. Kragten, J. M. Vohs, The oxidation of methanol to formaldehyde on TiO_2(110)-supported vanadia films, The Journal of Physical Chemistry B 105 (7) (2001) 1366–1373.

[14] T. Feng, J. Vohs, A TPD study of the partial oxidation of methanol to formaldehyde on CeO_2-supported vanadium oxide, Journal of Catalysis 221 (2) (2004) 619–629.

[15] R. Häggblad, J. B. Wagner, S. Hansen, A. Andersson, Oxidation of methanol to formaldehyde over a series of $fe_{1-x}al_x$v-oxide catalysts, Journal of Catalysis 258 (2) (2008) 345–355.

[16] X. Deng, D. C. Sorescu, J. Lee, Methanol oxidation to formaldehyde promoted at the step sites of ultrathin ZnO, Topics in Catalysis 61 (5) (2018) 499–508.

[17] F. Xu, W. Chen, C. A. Walenta, C. R. O'Connor, C. M. Friend, Dual lewis site creation for activation of methanol on Fe_3O_4 (111) thin films, Chemical Science 11 (9) (2020) 2448–2454.

[18] M. Merko, S. Delsing, G. Busser, M. Muhler, Non-oxidative dehydrogenation of methanol to formaldehyde over supported GaO_x-based catalysts, Journal of Catalysis 427 (2023) 115111.

[19] Ø. Borck, E. Schröder, First-principles study of the adsorption of methanol at the α-Al_2O_3 (0001) surface, Journal of Physics: Condensed Matter 18 (1) (2005) 1.

[20] Ø. Borck, E. Schröder, Adsorption of methanol and methoxy on the α-Cr_2O_3 (0001) surface, Journal of Physics: Condensed Matter 18 (48) (2006) 10751.

[21] M. M. Branda, G. R. Garda, H. A. Rodriguez, N. J. Castellani, Methanol decomposition on the β-Ga_2O_3 (100) surface: A DFT approach, Applied Surface Science 254 (1) (2007) 120–124, proceedings of the 13th International Conference on Solid Films and Surfaces.

[22] Z. Riguang, L. Hongyan, L. Lixia, L. Zhong, W. Baojun, A DFT study on the formation of CH_3O on Cu_2O (111) surface by CH_3OH decomposition in the absence or presence of oxygen, Applied Surface Science 257 (9) (2011) 4232–4238.

[23] Z. Liu, C. C. Sorrell, P. Koshy, J. N. Hart, DFT study of methanol adsorption on defect-free CeO_2 low-index surfaces, ChemPhysChem 20 (16) (2019) 2074–2081.

[24] R. G. S. Pala, H. Metiu, Selective promotion of different modes of methanol adsorption via the cation substitutional doping of a ZnO(101¯0) surface, Journal of Catalysis 254 (2) (2008) 325–331.

[25] G. K. Smith, S. Lin, W. Lai, A. Datye, D. Xie, H. Guo, Initial steps in methanol steam reforming on PdZn and ZnO surfaces: Density functional theory studies, Surface science 605 (7-8) (2011) 750–759.

[26] C. T. Vo, L. K. Huynh, J.-Y. Hung, J.-C. Jiang, Methanol adsorption and decomposition on ZnO (101¯0) surface: A density functional theory study, Applied surface science 280 (2013) 219–224.

[27] N. Abedi, P. Herrmann, G. Heimel, Methanol on ZnO ($10\overline{1}0$): From adsorption over initial dehydrogenation to monolayer formation, The Journal of Physical Chemistry C 119 (37) (2015) 21574–21584.

[28] S. Mehta, K. Joshi, From molecular adsorption to decomposition of methanol on various ZnO facets: A periodic DFT study, Applied Surface Science 602 (2022) 154150.

[29] Y.-F. Zhao, R. Rousseau, J. Li, D. Mei, Theoretical study of syngas hydrogenation to methanol on the polar Zn-terminated ZnO (0001) surface, The Journal of Physical Chemistry C 116 (30) (2012) 15952–15961.

[30] G. Kresse, O. Dulub, U. Diebold, Competing stabilization mechanism for the polar ZnO(0001)-Zn surface, Phys. Rev. B 68 (2003) 245409.

[31] D. J. Cooke, A. Marmier, S. C. Parker, Surface structure of $(10\overline{1}0)$ and $(11\overline{2}0)$ surfaces of ZnO with density functional theory and atomistic simulation, The Journal of Physical Chemistry B 110 (15) (2006) 7985–7991.

[32] P. E. Blöchl, Projector augmented-wave method, Physical Review B 50 (24) (1994) 17953–17979.

[33] G. Kresse, D. Joubert, From ultrasoft pseudopotentials to the projector augmented-wave method, Physical Review B 59 (3) (1999) 1758–1775.

[34] J. P. Perdew, K. Burke, M. Ernzerhof, Generalized gradient approximation made simple [phys. rev. lett. 77, 3865 (1996)], Physical Review Letters 78 (7) (1997) 1396–1396.

[35] G. Kresse, J. Hafner, *Ab initio* molecular-dynamics simulation of the liquid-metal–amorphous-semiconductor transition in germanium, Physical Review B 49 (20) (1994) 14251–14269.

[36] G. Kresse, J. Furthmüller, Efficient iterative schemes for *ab initio* total-energy calculations using a plane-wave basis set, Physical Review B 54 (16) (1996) 11169–11186.

[37] G. Kresse, J. Furthmüller, Efficiency of ab-initio total energy calculations for metals and semiconductors using a plane-wave basis set, Computational Material Science 6 (1) (1996) 15–50.

[38] A. Jain, S. P. Ong, G. Hautier, W. Chen, W. D. Richards, S. Dacek, S. Cholia, D. Gunter, D. Skinner, G. Ceder, K. A. Persson, Commentary: The

materials project: A materials genome approach to accelerating materials innovation, APL Materials 1 (1) (2013) 011002.

[39] R. R. Reeber, Lattice parameters of ZnO from 4.2° to 296°K, Journal of Applied Physics 41 (13) (1970) 5063–5066.

[40] E. M. Flores, M. L. Moreira, M. J. Piotrowski, Structural and electronic properties of bulk ZnX (X= O, S, Se, Te), ZnF_2, and ZnO/ZnF_2: A DFT investigation within PBE, PBE+ U, and hybrid HSE functionals, The Journal of Physical Chemistry A 124 (19) (2020) 3778–3785.

[41] D. Stradi, L. Jelver, S. Smidstrup, K. Stokbro, Method for determining optimal supercell representation of interfaces, Journal of Physics: Condensed Matter 29 (18) (2017) 185901.

[42] S. Grimme, Semiempirical GGA-type density functional constructed with a long-range dispersion correction, Journal of computational chemistry 27 (15) (2006) 1787–1799.

[43] R. Dronskowski, P. E. Blöchl, Crystal orbital hamilton populations (COHP): energy-resolved visualization of chemical bonding in solids based on density-functional calculations, The Journal of Physical Chemistry 97 (33) (1993) 8617–8624.

[44] V. L. Deringer, A. L. Tchougréeff, R. Dronskowski, Crystal orbital hamilton population (COHP) analysis as projected from plane-wave basis sets, The Journal of Physical Chemistry A 115 (21) (2011) 5461–5466.

[45] S. Maintz, V. L. Deringer, A. L. Tchougréeff, R. Dronskowski, Analytic projection from plane-wave and PAW wavefunctions and application to chemical-bonding analysis in solids, Journal of Computational Chemistry 34 (29) (2013) 2557–2567.

[46] S. Maintz, V. L. Deringer, A. L. Tchougréeff, R. Dronskowski, LOBSTER: A tool to extract chemical bonding from plane-wave based DFT, Journal of Computational Chemistry 37 (11) (2016) 1030–1035.

[47] T. M. Elmorsi, M. H. Elsayed, M. F. Bakr, Enhancing the removal of methylene blue by modified ZnO nanoparticles: kinetics and equilibrium studies, Canadian Journal of Chemistry 95 (5) (2017) 590–600.

[48] V. Venu Gopal, S. Kamila, Effect of temperature on the morphology of ZnO nanoparticles: a comparative study, Applied Nanoscience 7 (3) (2017) 75–82.